Systematic characterization of the conformation and dynamics of budding yeast chromosome XII

Benjamin Albert, Julien Mathon, Ashutosh Shukla, Hicham Saad, Christophe Normand, Isabelle Léger-Silvestre, David Villa, Alain Kamgoué, Julien Mozziconacci, Hua Wong, et al.

Systematic characterization of the conformation and dynamics of budding yeast chromosome XII

Benjamin Albert[1,2#], Julien Mathon[3#], Ashutosh Shukla[4], Hicham Saad[1,2], Christophe Normand[1,2], Isabelle Léger-Silvestre[1,2], David Villa[5], Alain Kamgoue [1,2], Julien Mozziconacci[6,7], Hua Wong[8], Christophe Zimmer[8], Purnima Bhargava [4*], Aurélien Bancaud[3,7*], and Olivier Gadal[1,2,7*]

Running title: Yeast chromosome organization.

eTOC summary statement: "Comprehensive analysis of the intranuclear territories and motion of budding yeast chromosome XII loci suggests that long range chromosome architecture is mainly determined by the physical principles of polymers".

Keywords : chromatin / ribosomal DNA / Nucleolus / nuclear architecture

1: LBME du CNRS ; 2 : Université de Toulouse, 118 route de Narbonne, F-31000 Toulouse, France.
3: CNRS, LAAS, 7 avenue du colonel Roche, F-31077 Toulouse, France
4 : Centre for Cellular and Molecular Biology, Council of Scientific and Industrial Research, Uppal Road, Hyderabad 500007, India
5: FRBT, Université de Toulouse, 118 route de Narbonne, F-31000 Toulouse, France.
6: Laboratory for Theoretical Physics of Condensed Matter, UPMC, 75005 Paris, France.
7: Groupement de recherche Architecture et Dynamique Nucléaire (GDR ADN)
8: Institut Pasteur, Unité d'Imagerie et Modélisation, 75015 Paris, France.
#these authors contributed equally to this work

* Corresponding authors:

Purnima Bhargava
email: purnima@ccmb.res.in
Phone: +33 (0)5 61 33 62 46; Fax: +33 (0)5 61 33 62 08 ;

Aurélien Bancaud
email: abancaud@laas.fr
Phone: +33 (0)5 61 33 62 46; Fax: +33 (0)5 61 33 62 08 ;

Olivier Gadal
email: gadal@biotoul.fr
Phone: +33(0)5 61 33 59 39; Fax: +33 (0)5 61 33 58 86;

Characters count: 19993
MS: 201208186, resubmission date 2013/05/17

Abstract (160 words)

Chromosome architecture is viewed as a key component of genes regulation, but principles of chromosomal folding and their relation with transcription remain elusive. Chromosome XII is the longest in the budding yeast genome and carries the ribosomal DNA (rDNA), which nucleates the nucleolar compartment, a major hallmark of nuclear organization. We used high-throughput live cell microscopy to characterize the conformation and dynamics of chromosome XII. We determined intranuclear territories of 15 loci distributed every ~100 kilobases along the chromosome and analyzed their motion over broad time scales (0.2-400 s). Loci territory positions were consistent with a computational model of chromosomes based on physically tethered polymers. A massive transcriptional reprogramming of the genome only marginally affected the chromosome XII internal large-scale organization. Finally, measured subdiffusive motions chromosome XII loci were consistent with the Rouse model from polymer physics, except at the rDNA. Our results suggest that global chromosome architecture is mainly determined by physical principles of polymers with local transcription-dependent effects.

Introduction

The genome of eukaryotes is organized in three-dimensions according to principles that remain poorly understood even in the yeast *S. cerevisiae* which is among the simplest models to study the organization of the eukaryotic nucleus. The 16 chromosomes of a haploid yeast exhibit a nonrandom spatial distribution, and three structural elements, namely centromeres (CEN), telomeres (TEL), and the nucleolus (NUC) have been identified as key players of their organization (Taddei and Gasser, 2012). The CEN are clustered near the spindle-pole body (SPB) (Guacci et al., 1994; Guacci et al., 1997; Jin et al., 1998; Jin et al., 2000). TEL are also clustered in foci at the nuclear envelope (NE) (Gotta et al., 1996; Klein et al., 1992), so that chromosome arms extend outwards from CEN to the periphery, defining a Rabl-like conformation (Jin et al., 2000). Diametrically opposed to the SPB, the NUC physically separates from the rest of the genome the repetitive rDNA genes carried on chromosome XII in a crescent-shaped structure of about one third of the nuclear volume (Léger-Silvestre et al., 1999; Yang et al., 1989).

The conformation of yeast chromosomes was analyzed using Chromosome Capture Conformation (3C) techniques (Dekker et al., 2002; Duan et al., 2010; Tanizawa et al., 2010), but without elucidating the mechanisms driving their folding (Langowski, 2011). Transcription may be involved in genome large scale architecture, given that the spatial position of some genes is correlated with their expression level (for review, see (Taddei and Gasser, 2012)). Actively transcribed genes could contact the NE, through nuclear pore complex interactions (Casolari et al., 2004; Schmid et al., 2006), and these interactions are driven by transcription in some cases (e.g. *GAL1-10* or *INO1*; (Brickner and Walter, 2004; Cabal et al., 2006; Casolari et al., 2004)). tRNA genes which are scattered throughout the

genome, appear to form foci at the nucleolar periphery (Thompson et al., 2003), as well as near the centromeres (Duan et al., 2010), but these results still remain the subject of discussions (Cournac et al., 2012; Witten and Noble, 2012). In fact, it is still unclear whether and how the positioning of specific genes impacts the long-range organization of chromosomes.

In this report, we studied the conformation and the dynamics of yeast chromosomes using high-throughput live cell microscopy, and to confront our results to recent computational model. We focused on the largest yeast chromosome (XII) because it contains the three classes of genes: the ribosomal DNA (rDNA) locus transcribed by Pol I and Pol III (Petes, 1979), ~600 protein coding genes transcribed by Pol II, and 22 ncRNA genes transcribed by Pol III. The chromosome XII was fluorescently labeled every 100 kb to produce a comprehensive description of position of one single yeast chromosome, showing a polymer-like conformation in agreement with the prediction of computational model based on polymer physics and volume exclusion (Wong et al., 2012). Some RNA polymerase III transcribed genes along chromosome XII deviate slightly from this model, while the global organization is not affected. We also investigated the contribution of transcription to chromosome conformation by inducing a modulation of transcription by TOR inhibition. This analysis showed that such major transcription reprogramming had little effect on chromosome XII conformation. Our study of chromosome architecture was finally extended to the analysis of the motion of different loci, which matches the predictions of polymer models, thus suggesting that the folding principles of yeast chromosomes are mainly dictated by polymer physics.

Results and discussion

Long range organization of chromosome XII between anchoring elements (TEL, CEN, NUC)

Global architecture of chromosome XII was first investigated in living yeast cells by monitoring the position of 15 loci distributed along the chromosome. Using targeted homologous recombination of fluorescent operator-repressor system (FROS), 12 independent insertions distributed every ~100 kb were generated along the non-rDNA region of chromosome XII (Fig. 1A). We also labeled three individual loci within the rDNA region at known distances from the CEN (Fig. 1; see Material and Methods).

We chose to represent the position of a locus as a probability distribution relative to nuclear and nucleolar centers in living cells (Berger et al., 2008; Therizols et al., 2010). The spatial repartition of loci positions was assayed in a large number of cells in interphase (>1500), and the data were represented in a color-coded statistical map of loci positions in which the percentage in an enclosing contour represents the probability to find a locus inside (Fig. 1B). The radius of the nuclei and their morphology, characterized by the distance between the nuclear and the nucleolar centers, were similar in all strains (see Fig. S1). We also selected FROS strains with comparable nuclear (3.4 +/- 0.09 μm^3) and nucleolar volumes (1.37 +/- 0.08 μm^3), so as to overlay the positions of loci in the same map (see Material and Methods and Movie 1).

The visual inspection of statistical maps shows that the position of loci along chromosome XII is consistent with a path dictated by the genomic coordinates of each locus and the segmentation of the chromosomes between three structuring elements CEN, TEL, and NUC (Fig. 1 B and movie 1). We then wished to assess whether chromosome XII folding could be predicted by nuclear models based on polymer physics (Wong et al., 2012). The median distance to the nuclear and nucleolar centers was plotted as a function of the genomic

coordinates of each locus (boxplots in Fig. 2A, B; see Material and Methods), and these data compared well with the model predictions (Wong et al., 2012)(black line in Fig. 2A, B). We noted that the fit to the model prediction was poorer for genomic positions 450-1050 kb, *i.e.* from NUC to the right TEL (see *e.g.* the anomalous dynamics of the rDNA in Fig. 4).

The smooth variations of the median positions between consecutive loci suggested that the statistical maps could be interpolated with a genomic resolution much finer than 100 kb. We thus computed statistical maps every kb along chromosome XII (movie 2; see Material and Methods), and we challenged their relevance by comparing them to the positions of four RNA polymerase III transcribed genes along chromosome XII (*tP(UGG), tA(UGC), tL(UAA)* and *SNR6*); their genomic positions correspond to the green boxplots of Fig. 2A and B. Experimental and interpolated statistical maps are represented in the upper half and lower half of Fig. 2C, respectively. If *SNR6* shows a good agreement with interpolation, mild or strong discrepancies are observed respectively for (tA(UGC); tL(UAA)) or (tP(UGG)). Such data argue for a local effect of Pol III genes on chromosome structure. However, this analysis is different from co-localization assays, in which Pol III transcribed genes were organized in clusters close to CEN or NUC (Duan et al., 2010; Thompson et al., 2003), but it suggests that the distribution of genes is primarily influenced by their genomic position, and only locally by sequence-specific physical interactions (Fig. 2 A, B). Note that we checked that the FROS insertion did not affect chromatin structure by analyzing the inner structure of *SNR6* using *in situ* Indirect-End Labeling (IEL; Fig. 2D). Our results show that nucleosomes positioning within the upstream and transcribed regions is similar in the control and the labeled strain (Fig. 2D). Moreover the transcription level of *SNR6* was not significantly modified by FROS labeling (Fig. 2D). In conclusion, experimental data and predictions from computational model are largely compatible, suggesting that the folding of chromosome XII is mainly dictated by local attachments to three main nuclear structures NUC, TEL, and CEN.

Major transcriptional reprogramming has little effect on chromosome XII structure

In order to investigate further whether molecular interactions driven by transcription played a role in global chromosome architecture, we probed the structure of chromosome XII by statistical mapping after a major transcriptional repression (Fig. 3) Cells were treated with rapamycin, an inhibitor of the conserved protein kinase complex TORC1 (Target of Rapamycine) (Loewith et al., 2002) which induces a global modification of transcription, mimicking nutrient deprivation characterized by transcriptional repression of Pol II ribosomal protein genes, rRNA 5S genes transcribed by Pol III, and a repression of Pol I activity (Hardwick et al., 1999; Wullschleger et al., 2006). After 20 min of rapamycin treatment, the mean nucleolar volume decreased by 37%, but the nucleus remained nearly constant in size (4% increase in volume) in agreement with previous studies (Therizols et al., 2010). The statistical maps of 12 loci positions were determined in non-treated *vs.* rapamycin treated cells, and are represented respectively in the upper half and lower half of each genemap (Fig. 3). Nucleolar size reduction generated a global shift of all loci toward the nucleolus. However, we did not detect major modifications of internal chromosome folding at the population level, thus supporting our model in which chromosome architecture is mainly determined by the biophysical properties of chromosomes and volume exclusion rather than by molecular interactions mediated by transcription.

Chromatin motion of chromosome XII

We investigated the dynamics of chromosome XII and confront these data to predictions of polymer models. The motion of 10 loci (marked with stars in Fig. 1A) was studied by recording their trajectories in 2D rather than in 3D, in order to increase the acquisition speed

and reduce photo-toxicity. Normal cell growth was observed during up to 2 hours of acquisition (movie 3). A broad temporal range (from 0.2 to 400 s) was probed using five distinct inter-frame intervals of 190, 360 ms for all loci, as well as 1, 1.5 and 10 s for three loci. A dedicated software was developed to perform systematic trajectory analysis (Fig. S2 A, B, C; See Material and Methods). This software allowed to extract the Mean Square Displacement (MSD) which is the average of the squared travel distances after a given time lag, for every locus, and to compare the dynamics in the case of central, peripheral, or nucleolar localized loci (Fig. S2). Trajectories during which deformations of the nucleus or detection of drifts of the nuclear center occurred (*e.g.* during mitosis, see movie 3) were disregarded.

Several studies suggested that chromatin motion was determined by a normal diffusive behavior in a restrained volume ($MSD \sim t$ in the small time limit, and $MSD \sim a$ in the long time limit with a the radius of constraint; (Heun et al., 2001; Marshall et al., 1997; Meister et al., 2010)). To display MSD in the short and long time regimes, we used linear and logarithmic representations (Fig. 4 and S3). Loci -30, 680 and rDNA were chosen as representative examples (Fig. 4). We observed that MSD curves exhibited a power-law scaling response expressed as $MSD \sim \Gamma . t^{\alpha}$ with the anomalous parameter α of ~ 0.5+/-0.07 (Fig. 4B) and the amplitude of the motion Γ ~0.01 $\mu m^2.s^{-0.5}$. Interestingly, the anomalous diffusive response is consistent with the Rouse polymer model that describes the movements of polymer segments based on their elastic interactions and on viscous frictions (De Gennes, 1979). This model is expected to apply to dense polymer solutions (De Gennes, 1979) and it was recently observed that the bacterial genome behaves as predicted from this model (Weber et al., 2010; Weber and Thierot, 2010). It also applies to the molecular dynamics simulations of the yeast genome (Rosa and Everaers, 2008), thus strengthening our view that chromosome properties in yeast fit with polymer models.

We further developed the description of chromatin dynamics at short time interval along chromosome XII. We compared the amplitude of the MSD traces by plotting Γ for every locus (Fig. 4C and Fig. S3), showing that the chromatin movements are homogeneous for most of the loci with a value in the range ~0.010-0.015 $\mu m^2.s^{-0.5}$. These results suggest a homogeneous behavior of chromatin throughout chromosome XII, except for rDNA. In addition, chromatin dynamics were not different for a locus with a central or peripheral localization (Fig. S3), and the amplitude of fluctuations Γ was moderately reduced by ~20% for loci with nucleolar *vs*. central localization (Fig. S3), suggesting that nucleolar proximity tends to restrain chromatin motion of non-rDNA loci. The investigation of MSD in the long time limit, best viewed in linear representation, revealed a deviation from the Rouse regime $MSD \sim \Gamma.t^{0.5}$. As previously suggested (Meister et al., 2010), the apparent confinement in the MSD is related to loci diffusing in a restrained volume. Space visited after 200s (~0.15 μm^2, ~0.25 μm^2, and ~0.3 μm^2 for the rDNA, locus -30 kb, and locus 680 kb, respectively), can be assigned to an explored volume of 0.57, 1.02, and 1.34 μm^3 for the three loci (Meister et al., 2010). These values are in excellent agreement with the dimensions of gene territories, as defined by the volume in which 50% of the gene positions are detected in statistical maps (Fig. 4D; rDNA, locus -30 kb, and locus 680 kb respectively at 0.8, 1.1 and 1.2 μm^3). This analysis also shows that one locus can explore the entire statistical map within few minutes.

Finally the motility of three chromosomal loci in the rDNA was investigated (Figure 4), showing a MSD with two distinct slopes: increasingly slowly for $t<5$ s ($\alpha \sim 0.25$) and more abruptly after 5 s ($\alpha \sim 0.7$). These dynamics are not consistent with the Rouse model (black line). In these polymer models several specific properties of the rDNA were disregarded, including among others the dynamics associated to transcriptional activity, the depletion of nucleosomes from actively transcribed rDNA (Conconi et al., 1989), or the possible local tethering of rDNA via CLIP proteins (Mekhail and Moazed, 2010; Mekhail et al., 2008). This

problem should be considered in future molecular dynamics simulations.

To conclude, our systematic analysis of position and motion of loci along chromosome XII showed that its inner structure mainly consists of constrained chromosome arms anchored to nuclear elements (SPB, NUC and NE), as expected from recent computational models (Tjong et al., 2012; Wong et al., 2012). We also demonstrated that the Rouse polymer model accurately describes the motion of chromatin loci except for the rDNA (Rosa and Everaers, 2008), the biophysical properties of which remain to be investigated.

We may finally speculate on whether the properties of chromosomes observed in yeast are relevant to metazoans. Our results suggest that chromosomes should be viewed as anchored polymers in a dense environment. Lamin associated domains (LAD) and nucleolar tethering domains (NAD), which appear to be distributed in large regions of the metazoan genome (Guelen et al., 2008; Németh et al., 2010; van Koningsbruggen et al., 2010), may provide anchoring regions analogous to NUC, CEN, and TEL. We foresee that the relevance of the Rouse model between anchoring regions should be studied, and spatial references should be proposed to construct statistical maps to investigate chromosome folding properties.

ACKNOWLEDGMENTS: This work was supported by an ATIP-plus grant from CNRS, by the Agence Nationale de la Recherche (Nucleopol, Ribeuc and programme JCJC), Jeune équipe from FRM, and University Paul Sabatier (J.M. Fellowship). This work is a French-Indian collaborative effort funded by IFCPAR Project 4103 between Dr Bhargava and Dr Gadal laboratories. We are gratefull to Mathieu Stouf, Héléne Badouin, Juliane Klehr and Céline Jeziorski for strains construction and initial characterization of loci positions. This work also benefited of the assistance of the imaging platform from Toulouse TRI.

Material and methods

Plasmid and yeast strains construction

pUC19-URA-iSCEI was constructed by cloning *Bam*HI-*Eco*RI fragment of the cut PCR product generated using oligonucleotide 1033-1034 and S288c genomic DNA into pUC19 at the same sites. Genotypes of the strains used in this study are described in supplementary Table S1. Oligonucleotides used for Polymerase Chain Reaction (PCR) are described in supplementary Table S2. *tetO* insertion were performed along the chromosome XII, every 10 kb in non-coding region. Genomic tetO integrations in non-rDNA regions were performed in two steps, first by integrating the *HIS3* or *URA3* gene by homologous recombination at the indicated location along chromosome arms, and second by inserting in the inserted markers (HIS3 or URA3) tetO repeats. Homologous recombination of *URA3* or *HIS3* was performed by transforming the PCR product amplified with appropriate oligonucleotides on pCR4-HIS3-M13 (Berger et al., 2008) or pSK-URA3-M13 (Berger et al., 2008) into TMS1-1a. After confirmation of the insertion site by PCR on genomic DNA, auxotrophic markers (*URA3* or *HIS3*) are used as target for insertion of *Eco*RI-linearized plasmids ptetO-NAT-his3Δ or ptetO-NAT-ura3Δ respectively. ptetO-NAT-his3Δ or ptetO-NAT-ura3Δ are bearing an array of 256 tetO, a Nourseothricin resistance marker and a yeast genome fragment allowing the insertion of the linearized plasmid by homologous recombination in HIS3 or URA3, as previously described (Berger et al., 2008; Rohner et al., 2008). The proper targeting of tetO site was confirmed by inactivation the auxotrophic markers, by size determination of chromosome XII by pulse-field gel electrophoresis (CHEF-DR® III, BIORAD), followed by southern blotting to confirm tetO insertion in the chromosome XII (Albert et al., 2011). Large chromosomal rearrangements, observed for some FROS labeled strains, were discarded by PFGE analysis. Number of rDNA repeats can change within a cell population, potentially

introducing heterogeneity amongst the FROS labeled clones (Pasero and Marilley, 1993), so we used PGFE to confirm that chromosome XII size was not altered in our labeled strains (data not shown).

Mapping FROS insertions in rDNA

Genomic tetO integrations in the rDNA regions were performed in two steps, first by integrating the *URA3* gene, bearing an adjacent I-*Sce*I site, by homologous recombination in one of the rDNA repeat, and second by inserting in the inserted *URA3* marker tetO repeats. The PCR product amplified with oligonucleotides 1035 and 1036 on pUC19-URA-iSCEI was transformed into TMS1-1a. To map rDNA insertion, I-*Sce*I genomic position was determined using pulse-field gel electrophoresis, followed by southern blotting to map tetO insertion. Following I-*Sce*I cleavage, FROS labeled chromosome XII is separated into a fragment containing left telomere and centromere and a region containing right telomere, revealed by EtBr staining. Southern blot using *tet*O as probe identified the right arm of the cleaved chromosome XII. We estimated insertion within the rDNA, at 750, 1060 and 1170 kb from the centromere-proximal edge of rDNA in clones rDNA-1, 2 and 3 respectively. Note that migration of a repeated genomic region, such as rDNA, is not strictly proportional to DNA size and insertion site was extrapolated considering 1.8 Mb of rDNA (about 200 repeats).

Chromatin structure using indirect end-labeling (IEL) and transcript quantification

Chromatin structure analysis by the Indirect-end-labeling (IEL) method, RNA extraction and quantification were performed as described (Arimbasseri and Bhargava, 2008), and repeated at least three times for each experiment. Briefly, for IEL analysis, yeast cells were

spheroplasted and subjected to partial digestion with micrococcal nuclease. DNA was extracted, digested with *Hind*III, resolved on 1.5% agarose gel and Southerm transferred. Probe for hybridization was amplified using oligonucleotides described in supplementary table S2 and α-[^{32}P]-ATP in a PCR reaction. A 1kb radiolabeled DNA ladder was run on the same gel as size marker. Primer extension on RNA extracted from FROS tagged and untagged strains to get cDNA preparation, was done by using radio-labeled primers. Products were resolved on 8 M urea–10% polyacrylamide gel, bands were visualized by phosphorimaging and *SNR6* transcript was quantified by using Image gauge (Fuji) software as described earlier (Arimbasseri and Bhargava, 2008)(Shivaswamy et al., 2004).

Fluorescence microscopy of living yeast cells

Yeast media were used as previously described (Rose et al., 1990). YPD is made of 1% yeast extract, 2% peptone and 2% dextrose. SC is made of 0.67% nitrogene base w/o amino acids (BD Difco, USA), 2 % dextrose supplemented with amino acids mixture (AA mixture Bio101, USA), adenine and uracil. Cells were grown overnight at 30 °C in YPD. Cells were diluted at 10^6 cells/ml, and were harvested when OD600 reached 4.10^6 cells/ml and rinsed twice with the corresponding SC media. Cells were spread on slides coated with a SC media patch containing 2% agarose and 2% glucose. Cover slides were sealed with "VaLaP" (1/3 vaseline, 1/3 lanoline, 1/3 paraffin). For long time-lapse acquisition and confocal imaging, imaging chamber were thermostated at 30°C.

Microscope image acquisition

Confocal Microscopy was limited to 20 min after mounting and performed with an Andor Revolution Nipkow-disk confocal system installed on a Olympus IX-81, featuring a CSU22 confocal spinning disk unit (Yokogawa) and an EMCCD camera (DU 888, Andor). The system was controlled using the mode "Revolution FAST" of Andor Revolution IQ1 software (Andor). Images were acquired using an Olympus 100x objective (Plan APO, 1.4 NA, oil immersion). Single laser lines used for excitation were diode pumped solid state lasers (DPSSL) exciting GFP fluorescence at 488 nm (50 mW, Coherent) and mCherry fluorescence at 561 nm (50 mW, Cobolt jive), a Semrock bi-bandpass emission filter (Em01-R488/568-15) allowed collection of green and red fluorescence. Pixel size was 65 nm. For 3D analysis, Z-stacks of 41 images with a 250-nm Z-step were used. Exposure time was 200 ms.

MSD analysis was carried out by recording the movements of chromosome loci by epi-fluorescence on two different microscope setting, depending on inter-frame interval. For long time intervals (1.5s, 4s and 10 s), image acquisition was performed on a Ti-E/B inverted microscope (Nikon) equipped with Perfect Focus System (PFS), suitable for long-range time-lapse experiments. The system was equipped with a 100 X oil immersion objective (CFI Plan fluor 100X, ON 1.30, Dt0.2), HG Intensilight illumination with low power (NDFilter=6.3 for GFP; 3.0 for mCherry), filter cubes TE/ZP FITC (FITC-3540C; semrock) for GFP signal and TE/ZP TEXAS RED (TxRed-4040C; Semrock) for mCherry imaging, 1.5 X lens and an EMCCD camera (Andor DU-897; EM gain 555 GFP; 40 for mCherry). Measured pixel size was 106.7 nm. Acquisition was set to 300 ms or 600 ms respectively for GFP and mCherry. For short time intervals (50 and 200 ms), imaging was performed using a BX-51 upright microscope (Olympus) equipped with a laser diode light source (Lumencor), a 100X oil immersion objective (NA=1.4), and an EMCCD camera (Andor DU-897), as described in (Hajjoul et al., 2009). The GFP excitation emission at 470+/-10 nm was set to 7.53 W/μm^2.

For short time intervals (50 and 200 ms), time-lapse sequences consisted in 300 consecutive images, and we displayed MSD traces on 150 time intervals in order to ensure the statistical relevance of mean displacements. mCherry signal was recorded at the end of GFP acquisition. For longer time intervals (1.5s; 4s and 10s interframe), time lapse images were acquired respectively for 5, 15 and 120 min, and manually checked to discard drifting cells. For GFP exposure with inter-frame of 10s, mCherry and brightfield acquisition was performed every 100s (each 10 GFP frames) to limit phototoxicity.

Image processing for time-lapse movie

Movie 3 file was generated by NIS image (Nikon), and was imported into final cut pro X (Apple). Color enhancement and dust attenuation was obtained by background correction. Timeline and scale bar were inserted in the movie file using Adobe Flash CS5 Professional (Adobe).

Image analysis for locus position

Confocal images were processed and analyzed with a Matlab script nucloc, available at http://www.nucloc.org/ (MathWorks) (Berger et al., 2008). Boxplot of nuclear radius, nuclear-nucleolar center distances were generated using boxplot function (Matlab). Boxplot of median distances to nuclear center, nucleolar center were computed in two steps, by first calculating median distances for each 100 nuclei, and then plotting boxplot of the median values obtained.

Image analysis for gene trajectory

Automatic particle tracking and spatial registration in time lapse analysis was then performed with our custom-made software run in MatLab. Single particle tracking software built on the MTT platform (Serge et al., 2008) was developed to perform high-throughput 2D trajectory analysis over a large temporal range. For trajectory analysis, we first evaluated the variations of the positioning error with the signal-to-noise ratio (SNR) in order to compensate for biases associated to the difference in brightness between the different strains (Fig. S2). Objects of controlled brightness and position were generated *in silico*, and tracked with our algorithm to retrieve the detection error, which was in the range 5.10^{-4}-10^{-5} μm^2. Due to the very high accuracy of gene position determination, correcting nuclear motion from gene trajectory added noise to observed motion. Rather than a systematic correction for nuclear center, we then manually excluded gene trajectories with detectable motion of nuclear position, leading to exclusion of <10% of trajectories for short time lapse, and 30-50% of trajectories for long-time lapse. Gene movements were recorded at fast or slow acquisition rates, resulting in different SNR, hence in different tracking error SNR. Starting from raw data, we compensated for the difference in SNR by adding an error to the slow acquisition MSD dataset, which is determined by the difference in tracking precision. Datasets are then fused and filtered using a Gaussian filter (order 11) (see Fig. 2). The resulting dataset is adjusted with an anomalous diffusion model. MSD curves were ultimately extracted and analyzed using Igor Pro (WaveMetrics).

Online supplemental material:

Genotypes of the strains used in this study are described in supplementary Table S1. Oligonucleotides are described in supplementary Table S2, plasmids used are described in supplementary Table S3.

Videos show overlaid color-coded statistical mapping of loci positions (Movie 1), interpolation between color-coded statistical mapping of loci positions (Movie 2) and time-lapse series of the 90kb locus labeled strain (Movie 3).

Supplementary figures depict nuclear morphology of the 31 analyzed populations (Fig. S1), Methods used for tracking genes in living cells. (Fig. S2) and MSD responses for loci -136, -80, CEN, 90 and 170 kb along chromosome XII (Fig. S3).

Codes (matlab scripts) of custom made software tracking loci are available as .Zip file as supplemental material hosted at www.jcb.org. Executable files are available upon request.

References :

Albert, B., I. Leger-Silvestre, C. Normand, M.K. Ostermaier, J. Perez-Fernandez, K.I. Panov, J.C. Zomerdijk, P. Schultz, and O. Gadal. 2011. RNA polymerase I-specific subunits promote polymerase clustering to enhance the rRNA gene transcription cycle. *J Cell Biol*. 192:277-293.

Arimbasseri, A.G., and P. Bhargava. 2008. Chromatin structure and expression of a gene transcribed by RNA polymerase III are independent of H2A.Z deposition. *Mol Cell Biol*. 28:2598-2607.

Berger, A.B., G.G. Cabal, E. Fabre, T. Duong, H. Buc, U. Nehrbass, J.C. Olivo-Marin, O. Gadal, and C. Zimmer. 2008. High-resolution statistical mapping reveals gene territories in live yeast. *Nat Methods*. 5:1031-1037.

Brickner, J.H., and P. Walter. 2004. Gene recruitment of the activated INO1 locus to the nuclear membrane. *PLoS Biol*. 2:e342.

Cabal, G.G., A. Genovesio, S. Rodriguez-Navarro, C. Zimmer, O. Gadal, A. Lesne, H. Buc, F. Feuerbach, J. Olivo-Marin, E. Hurt, and U. Nehrbass. 2006. SAGA interacting factors confine sub-diffusion of transcribed genes to the nuclear envelope. *Nature*. 441:770-773.

Casolari, J.M., C.R. Brown, S. Komili, J. West, H. Hieronymus, and P.A. Silver. 2004. Genome-wide localization of the nuclear transport machinery couples transcriptional status and nuclear organization. *Cell*. 117:427-439.

Conconi, A., R.M. Widmer, T. Koller, and J.M. Sogo. 1989. Two different chromatin structures coexist in ribosomal RNA genes throughout the cell cycle. *Cell*. 57:753-761.

Cournac, A., H. Marie-Nelly, M. Marbouty, R. Koszul, and J. Mozziconacci. 2012. Normalization of a chromosomal contact map. *BMC Genomics*. 13:436.

De Gennes, P.G. 1979. Scaling Concepts in Polymer Physics Cornell University Press.

Dekker, J., K. Rippe, M. Dekker, and N. Kleckner. 2002. Capturing chromosome conformation. *Science*. 295:1306-1311.

Duan, Z., M. Andronescu, K. Schutz, S. McIlwain, Y.J. Kim, C. Lee, J. Shendure, S. Fields, C.A. Blau, and W.S. Noble. 2010. A three-dimensional model of the yeast genome. *Nature*. 465:363-367.

Gotta, M., T. Laroche, A. Formenton, L. Maillet, H. Scherthan, and S.M. Gasser. 1996. The clustering of telomeres and colocalization with Rap1, Sir3, and Sir4 proteins in wild-type Saccharomyces cerevisiae. *J Cell Biol*. 134:1349-1363.

Guacci, V., E. Hogan, and D. Koshland. 1994. Chromosome condensation and sister chromatid pairing in budding yeast. *J Cell Biol*. 125:517-530.

Guacci, V., E. Hogan, and D. Koshland. 1997. Centromere position in budding yeast: evidence for anaphase A. *Mol Biol Cell*. 8:957-972.

Guelen, L., L. Pagie, E. Brasset, W. Meuleman, M.B. Faza, W. Talhout, B.H. Eussen, A. de Klein, L. Wessels, W. de Laat, and B. van Steensel. 2008. Domain organization of human chromosomes revealed by mapping of nuclear lamina interactions. *Nature*. 453:948-951.

Hajjoul, H., S. Kocanova, I. Lassadi, K. Bystricky, and A. Bancaud. 2009. Lab-on-Chip for fast 3D particle tracking in living cells. *Lab Chip*. 9:3054-3058.

Hardwick, J.S., F.G. Kuruvilla, J.K. Tong, A.F. Shamji, and S.L. Schreiber. 1999. Rapamycin-modulated transcription defines the subset of nutrient-sensitive signaling

pathways directly controlled by the Tor proteins. *Proc Natl Acad Sci U S A*. 96:14866-14870.

Heun, P., T. Laroche, K. Shimada, P. Furrer, and S.M. Gasser. 2001. Chromosome dynamics in the yeast interphase nucleus. *Science*. 294:2181-2186.

Jin, Q., E. Trelles-Sticken, H. Scherthan, and J. Loidl. 1998. Yeast nuclei display prominent centromere clustering that is reduced in nondividing cells and in meiotic prophase. *J Cell Biol*. 141:21-29.

Jin, Q.W., J. Fuchs, and J. Loidl. 2000. Centromere clustering is a major determinant of yeast interphase nuclear organization. *J Cell Sci*. 113:1903-1912.

Klein, F., T. Laroche, M.E. Cardenas, J.F. Hofmann, D. Schweizer, and S.M. Gasser. 1992. Localization of RAP1 and topoisomerase II in nuclei and meiotic chromosomes of yeast. *J Cell Biol*. 117:935-948.

Langowski, J. 2011. Chromosome conformation by crosslinking: Polymer physics matters. *Nucleus*. 1:37-39.

Léger-Silvestre, I., S. Trumtel, J. Noaillac-Depeyre, and N. Gas. 1999. Functional compartmentalization of the nucleus in the budding yeast Saccharomyces cerevisiae. *Chromosoma*. 108:103-113.

Loewith, R., E. Jacinto, S. Wullschleger, A. Lorberg, J.L. Crespo, D. Bonenfant, W. Oppliger, P. Jenoe, and M.N. Hall. 2002. Two TOR complexes, only one of which is rapamycin sensitive, have distinct roles in cell growth control. *Mol Cell*. 10:457-468.

Marshall, W.F., A. Straight, J.F. Marko, J. Swedlow, A. Dernburg, A. Belmont, A.W. Murray, D.A. Agard, and J.W. Sedat. 1997. Interphase chromosomes undergo constrained diffusional motion in living cells. *Curr Biol*. 7:930-939.

Meister, P., L.R. Gehlen, E. Varela, V. Kalck, and S.M. Gasser. 2010. Visualizing yeast chromosomes and nuclear architecture. *Methods Enzymol*. 470:535-567.

Mekhail, K., and D. Moazed. 2010. The nuclear envelope in genome organization, expression and stability. *Nat Rev Mol Cell Biol*. 11:317-328.

Mekhail, K., J. Seebacher, S.P. Gygi, and D. Moazed. 2008. Role for perinuclear chromosome tethering in maintenance of genome stability. *Nature*. 456:667-670.

Németh, A., A. Conesa, J. Santoyo-Lopez, I. Medina, D. Montaner, B. Péterfia, I. Solovei, T. Cremer, J. Dopazo, and G. Längst. 2010. Initial genomics of the human nucleolus. *PLoS Genet*. In press.

Pasero, P., and M. Marilley. 1993. Size variation of rDNA clusters in the yeasts Saccharomyces cerevisiae and Schizosaccharomyces pombe. *Mol Gen Genet*. 236:448-452.

Petes, T.D. 1979. Yeast ribosomal DNA genes are located on chromosome XII. *Proc Natl Acad Sci U S A*. 76:410-414.

Rohner, S., S.M. Gasser, and P. Meister. 2008. Modules for cloning-free chromatin tagging in Saccharomyces cerevisae. *Yeast*. 25:235-239.

Rosa, A., and R. Everaers. 2008. Structure and dynamics of interphase chromosomes. *PLoS Comput Biol*. 4:e1000153.

Rose, M.D., F. Winston, and P. Hieter. 1990. Methods in Yeast Genetics. A Laboratory Manual. Cold Spring Harbor, NY,.

Schmid, M., G. Arib, C. Laemmli, J. Nishikawa, T. Durussel, and U.K. Laemmli. 2006. Nup-PI: the nucleopore-promoter interaction of genes in yeast. *Mol Cell*. 21:379-391.

Serge, A., N. Bertaux, H. Rigneault, and D. Marguet. 2008. Dynamic multiple-target tracing to probe spatiotemporal cartography of cell membranes. *Nat Methods*. 5:687-694.

Shivaswamy, S., G.A. Kassavetis, and P. Bhargava. 2004. High-level activation of transcription of the yeast U6 snRNA gene in chromatin by the basal RNA polymerase III transcription factor TFIIIC. *Mol Cell Biol*. 24:3596-3606.

Taddei, A., and S.M. Gasser. 2012. Structure and function in the budding yeast nucleus. *Genetics*. 192:107-129.

Tanizawa, H., O. Iwasaki, A. Tanaka, J.R. Capizzi, P. Wickramasinghe, M. Lee, Z. Fu, and K. Noma. 2010. Mapping of long-range associations throughout the fission yeast genome reveals global genome organization linked to transcriptional regulation. *Nucleic Acids Res*. 38:8164-8177.

Therizols, P., T. Duong, B. Dujon, C. Zimmer, and E. Fabre. 2010. Chromosome arm length and nuclear constraints determine the dynamic relationship of yeast subtelomeres. *Proc Natl Acad Sci U S A*. 107:2025-2030.

Thompson, M., R.A. Haeusler, P.D. Good, and D.R. Engelke. 2003. Nucleolar clustering of dispersed tRNA genes. *Science*. 302:1399-1401.

Tjong, H., K. Gong, L. Chen, and F. Alber. 2012. Physical tethering and volume exclusion determine higher-order genome organization in budding yeast. *Genome research*.

van Koningsbruggen, S., M. Gierlinski, P. Schofield, D. Martin, G.J. Barton, Y. Ariyurek, J.T. den Dunnen, and A.I. Lamond. 2010. High-resolution whole-genome sequencing reveals that specific chromatin domains from most human chromosomes associate with nucleoli. *Mol Biol Cell*. 21:3735-3748.

Weber, S.C., A.J. Spakowitz, and J.A. Theriot. 2010. Bacterial chromosomal loci move subdiffusively through a viscoelastic cytoplasm. *Phys Rev Lett*. 104:238102.

Weber, S.C., and J.A.S. Thierot, A. J. 2010. Subdiffusive motion of a polymer composed of subdiffusive monomers. *Phys Rev E*. 82:011913.

Witten, D.M., and W.S. Noble. 2012. On the assessment of statistical significance of three-dimensional colocalization of sets of genomic elements. *Nucleic Acids Res*. 40:3849-3855.

Wong, H., H. Marie-Nelly, S. Herbert, P. Carrivain, H. Blanc, R. Koszul, E. Fabre, and C. Zimmer. 2012. A predictive computational model of the dynamic 3D interphase yeast nucleus. *Curr Biol*. 22:1881-1890.

Wullschleger, S., R. Loewith, and M.N. Hall. 2006. TOR signaling in growth and metabolism. *Cell*. 124:471-484.

Yang, C.H., E.J. Lambie, J. Hardin, J. Craft, and M. Snyder. 1989. Higher order structure is present in the yeast nucleus: autoantibody probes demonstrate that the nucleolus lies opposite the spindle pole body. *Chromosoma*. 98:123-128.

FIGURE LEGENDS

Figure 1. Color-coded statistical mapping of positions of fifteen loci along chromosome XII. **A** Schematic representation of chromosome XII with the 15 FROS labeled loci. Note that the rDNA of 1.8 Mb is depicted as a 1 Mb segment. Loci studied by particle tracking are marked with a star. **B** Spatial distributions of each locus are represented using genemap, a color-coded heat map determined by the percentile of the distribution (Berger et al., 2008; Therizols et al., 2010). In the upper panel the dashed yellow circle, the red curve, and small red circle respectively depict the median nuclear envelope, the median nucleolus, and the median location of the nucleolar center. In the lower panel the genemaps are represented with the genomic position indicated on top (N represents the number of nuclei analyzed). Note that the position along the genome of the 3 rDNA loci has been determined by *I-SceI* cleavage. The data shown are from a single representative experiment out of three repeats.

Figure 2. The position of loci along chromosome XII relative to the nucleolus (NUC) and the nuclear envelope (NE) are predicted by computational modelling. Distance of the locus to the nuclear center (**A)** and to the nucleolar center (**B**) is plotted *vs*. its genomic position. Yellow and red ellipsoids respectively depict nuclear envelope and nucleolus and the black line represents the distance (left panel). The median distance is shown with boxplots for the 15 loci described in figure 1 and for four RNA polymerase III genes (white and green datasets). Median distance of chromosome XII loci to nuclear center and to centroid of rDNA segment from a computational model of chromosome XII (Wong et al., 2012) is shown in solid black line. **C** Genemap of loci t(P(UGG)L, tA(UGC)L, SNR6 and t(L(UAA)L relative to interpolated positions -58, 65, 216 and 647 kb (which correspond to their genomic coordinates) reveals global agreement between model and measurements (see movie 2). Genemap

experimentally determined (upper panel) is compared to interpolated position (lower panel). **D** The yeast U6 snRNA gene *SNR6* is unaffected by FROS insertion. Locations of important elements are indicated relative to the transcriptional start site (bent arrow) as +1 (upper part). Indirect end-labeling analysis of the chromatin structure on *SNR6* is shown in the lower-right panel. Ellipses on the right-hand side mark the positioned nucleosomes in the corresponding lanes with wild-type unmodified (U) or FROS tagged (T) strains. Note the apparent hyper-sensitive site (*) detected upon FROS insertion correspond to an *Hind*III site introduced along with *tet*O repeat. *SNR6* expression is not affected by FROS insertion. Transcript levels in untagged and FROS tagged strains were normalized against the U4 transcript used as an internal control. Average and scatter of RNA levels estimated from three independent experiments are plotted (lower-left panel).

Figure 3. Color-coded statistical mapping of positions of twelve loci along chromosome XII after rapamycin treatment. **A** Schematic representation of chromosome XII with the 12 FROS labeled loci using the centromere as origin. **B** The spatial distributions of each locus (lower part of the genemap representations) is compared to loci position in rapamycin treated cells (upper part of the genemap representations).

Figure 4. Loci motion is slowed down at NUC, and homogeneous elsewhere. **A** The temporal evolution of the MSD is plotted at position 680 kb, -30kb (for central localization) and at rDNA (nucleolar localization) in log-log (upper panel) or linear (lower panel) scale. MSD extracted from time lapse of 0.19, 0.36, 1, 1.5 and 10s interframes are depicted in different colors. The curves are fitted with an anomalous diffusion model (solid lines), showing that the anomaly parameter is 0.5+/-0.07. Note that the movements of rDNA are slow in comparison

to that of the locus at 680 or -30 kb. The black line represents the fit to the dataset with a power-law scaling of 0.55. **B** The plot represents the anomaly parameter *vs*. the genomic position, and shows the different dynamics in NUC for the 10 analyzed loci. **C** Spatial fluctuations of the 10 analyzed loci are compared by measuring the amplitude of the power law scaling response using a model with $\Gamma t^{0.5}$. **D** The gene territory, defined by the volume occupied by 50 percent of the gene population (the green isocontour in genemaps) expressed in μm^3, is measured as a function of the genomic position. Gene territories experimental errors were determined by measuring gene territories from three samplings of the full dataset.

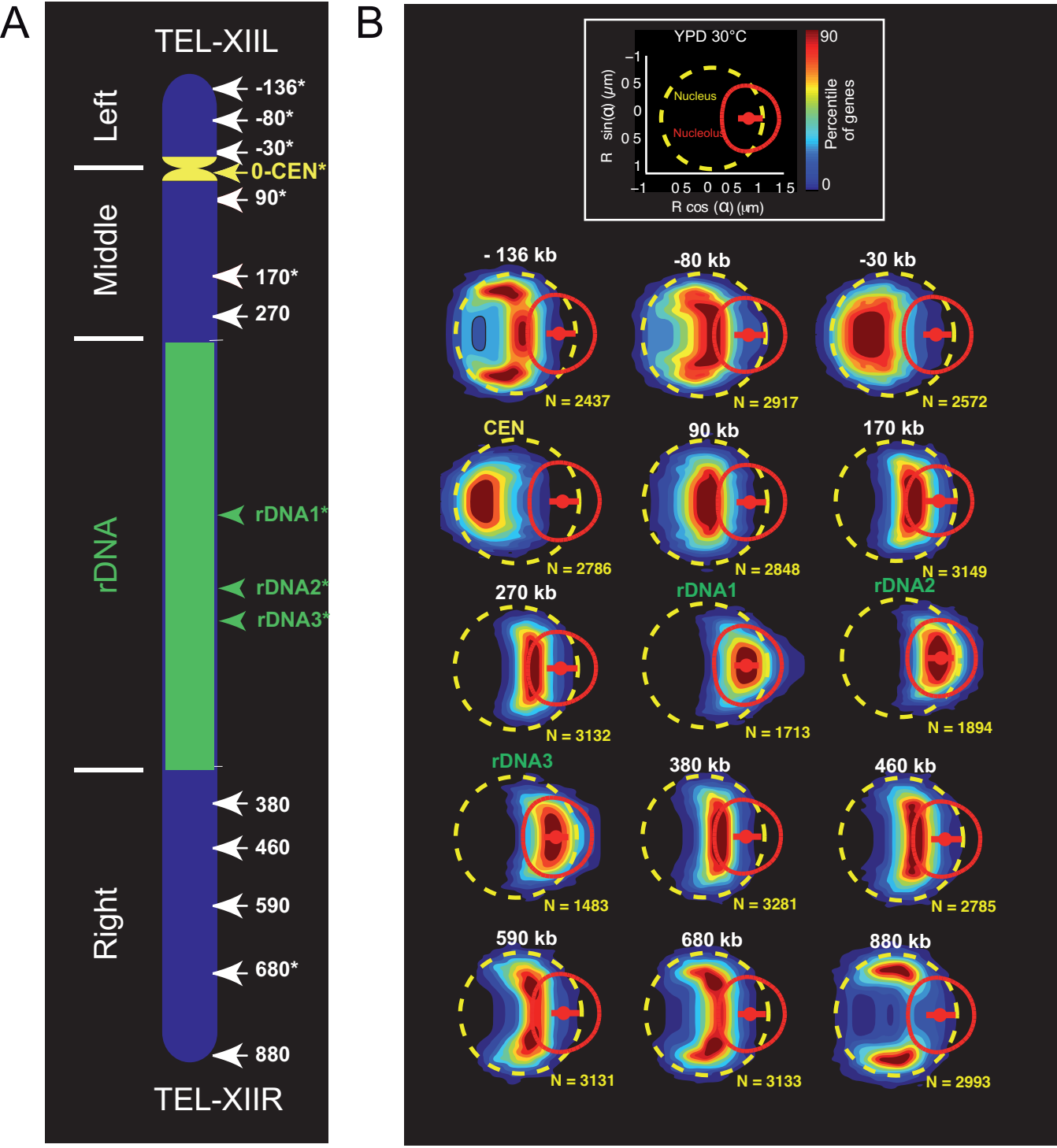

Figure 1- Albert et al.,

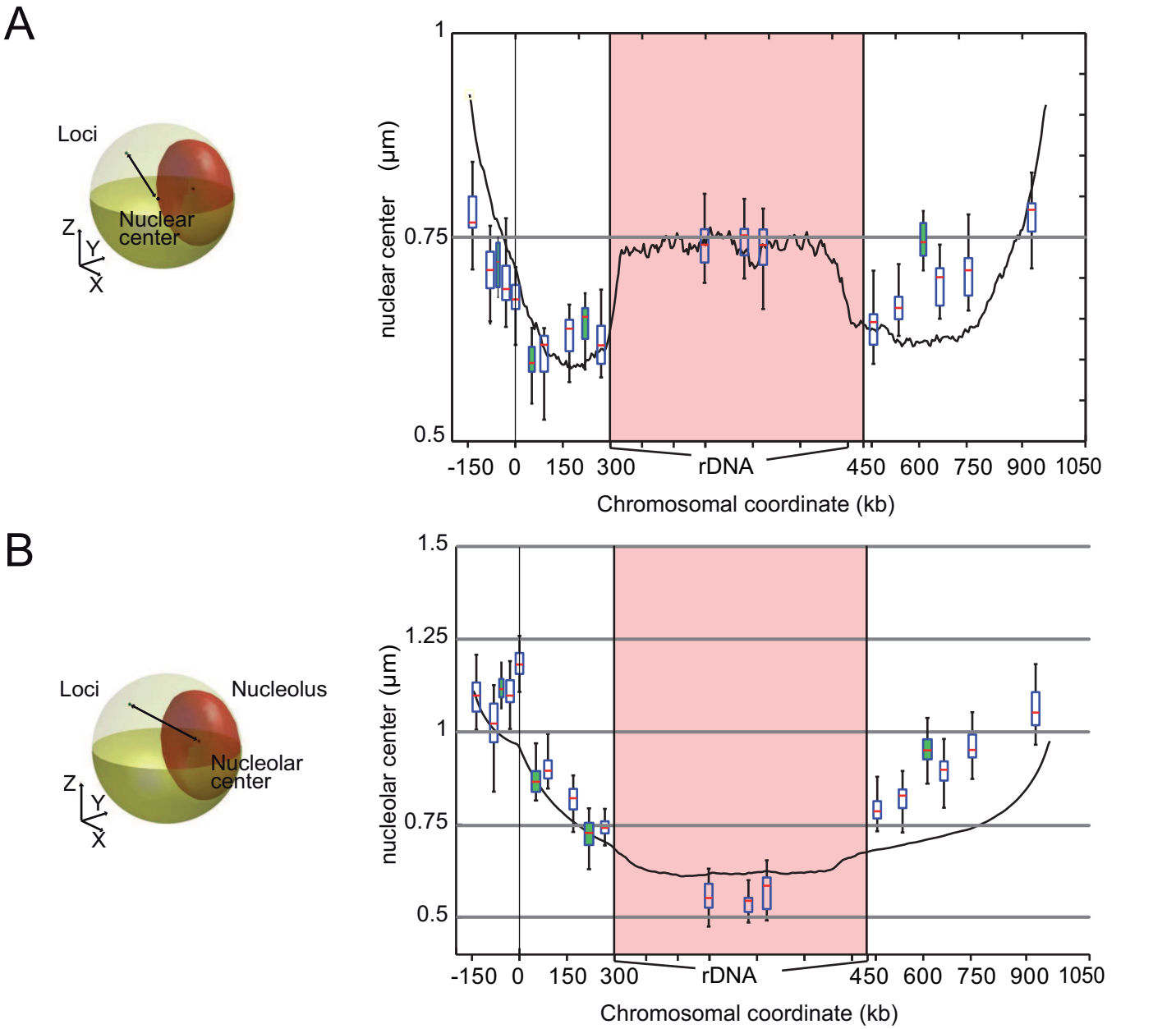

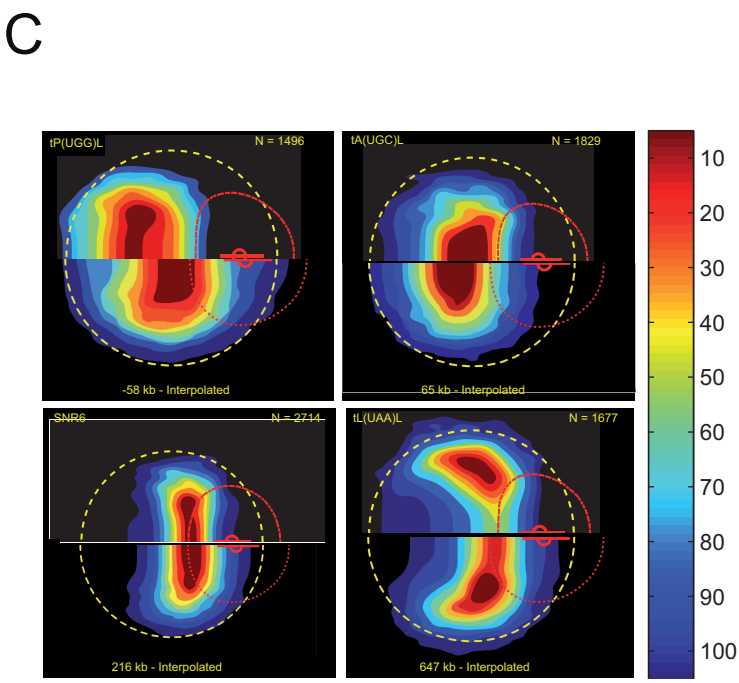

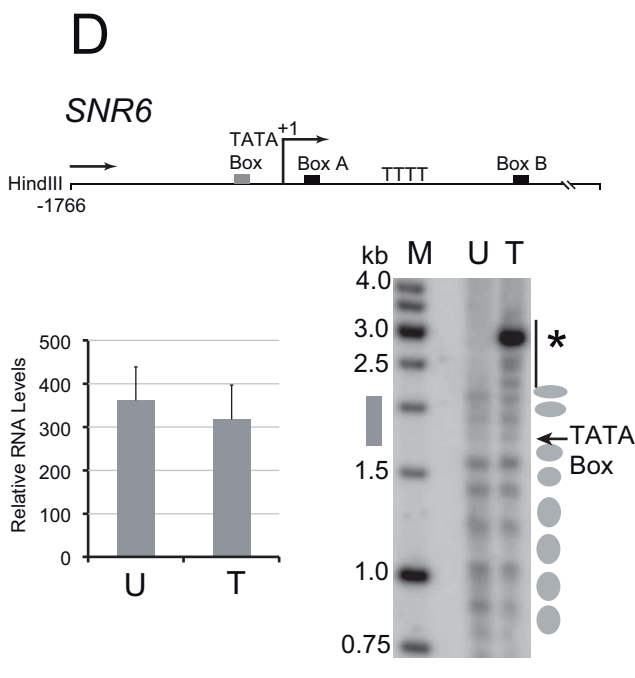

Figure 2 - Albert et al.,

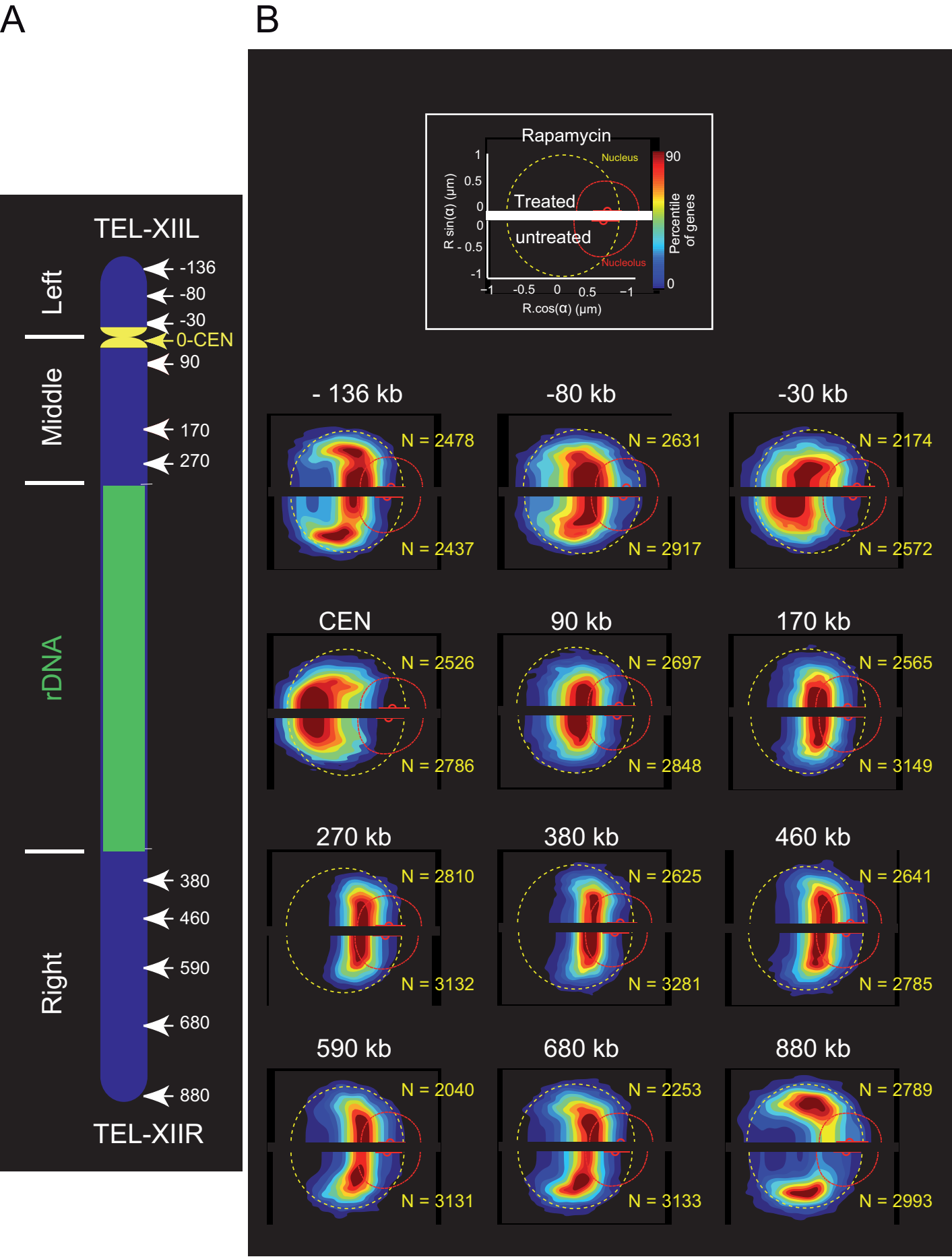

Figure 3- Albert et al.,

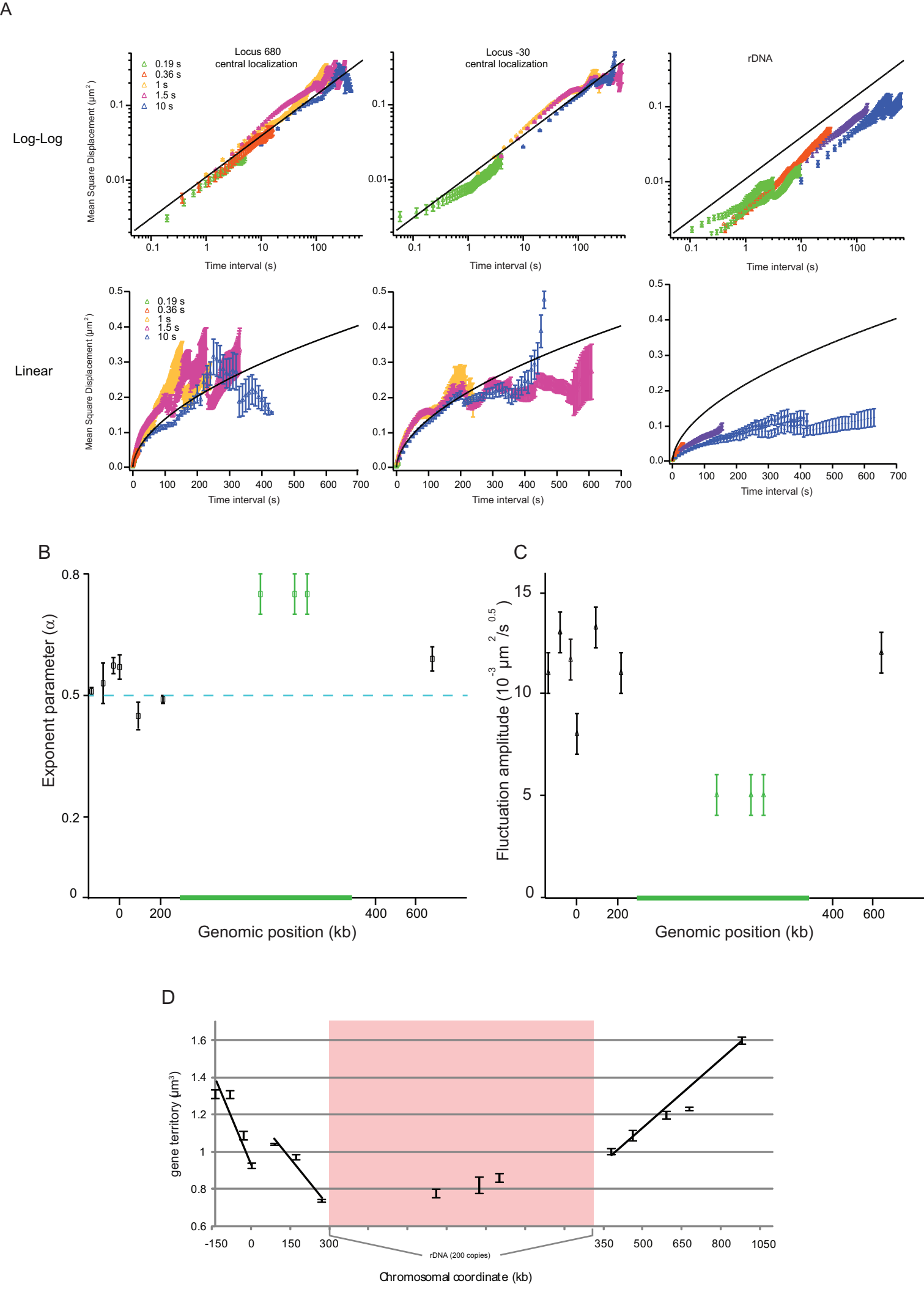

Figure 4- Albert et al.,

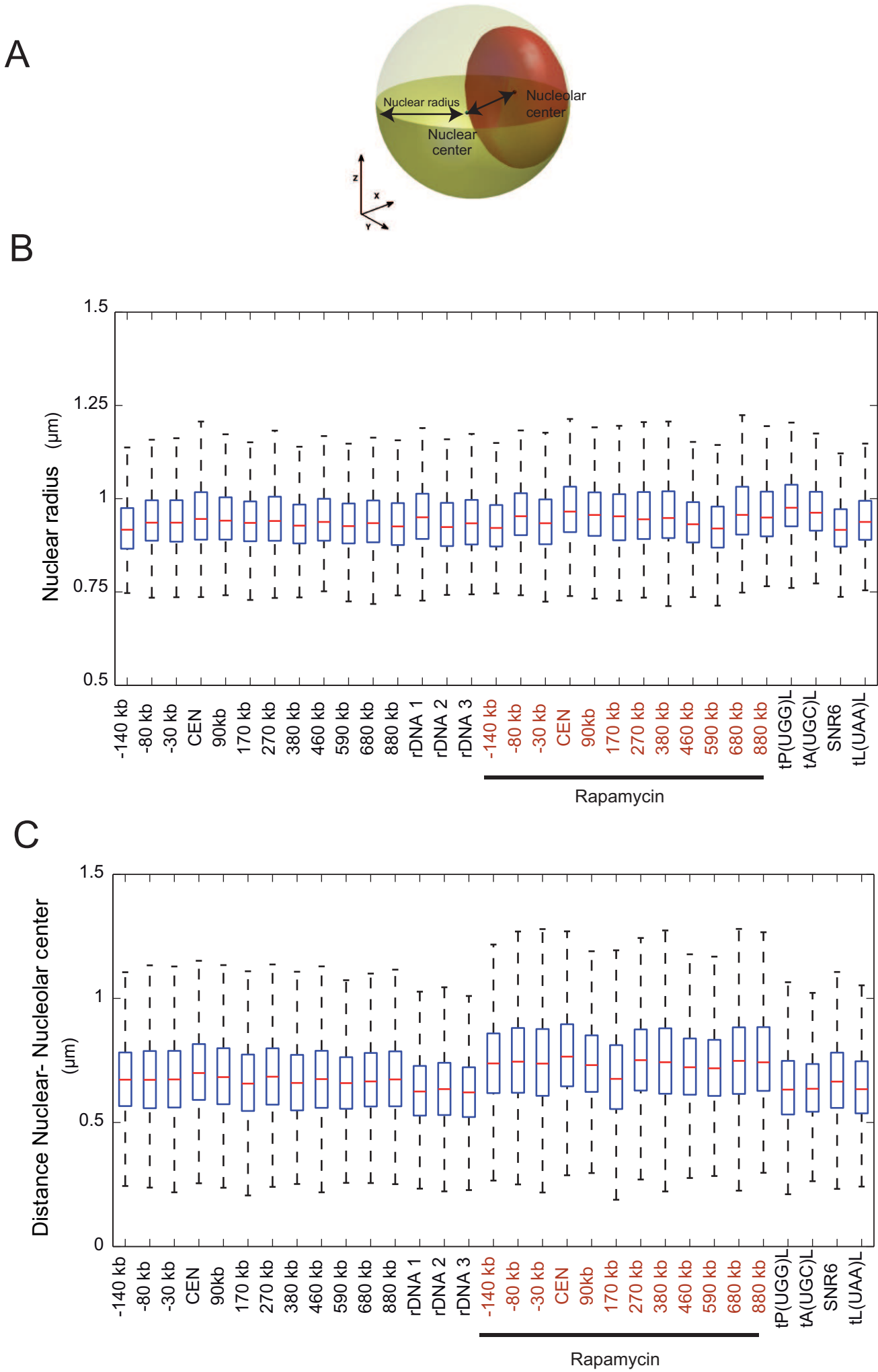

Supplementary figure 1 ; Albert et al.,

A

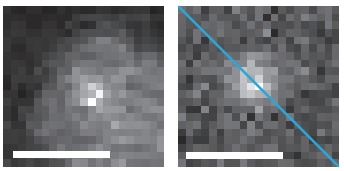

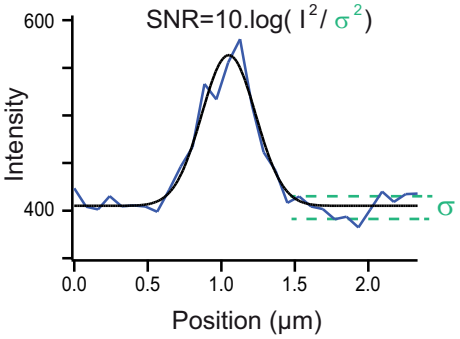

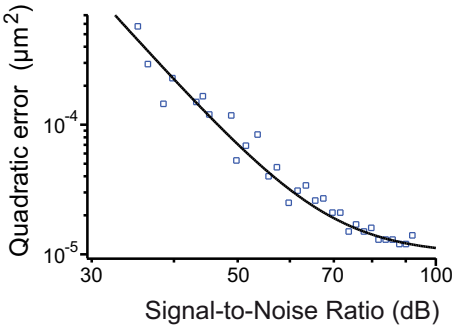

B

Position	SNR (dB) 60 ms	SNR (dB) 200 ms
-136	46 +/- 2	58 +/- 7
-80	65 +/- 3	72 +/- 6
-30	60 +/- 2	72 +/- 5
0	40 +/- 2	68 +/- 15
90	41 +/- 2	59 +/- 5
170	45 +/- 2	49+/- 3
rDNA1	83 +/- 9	80 +/- 8
rDNA2	83 +/- 7	79 +/- 6
rDNA3	83 +/- 9	80 +/- 9
680	33 +/- 2	53 +/- 6

C

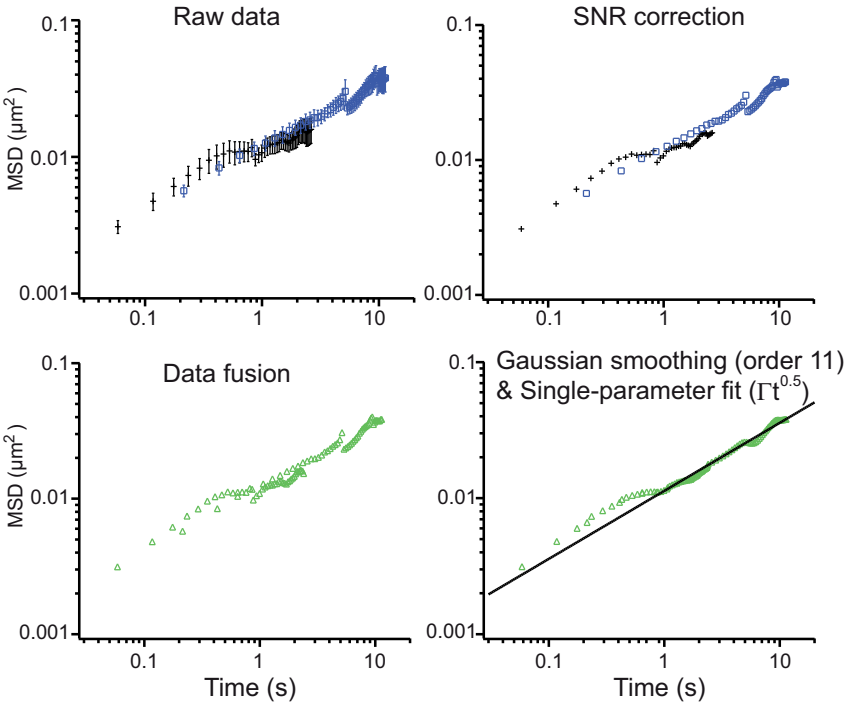

D

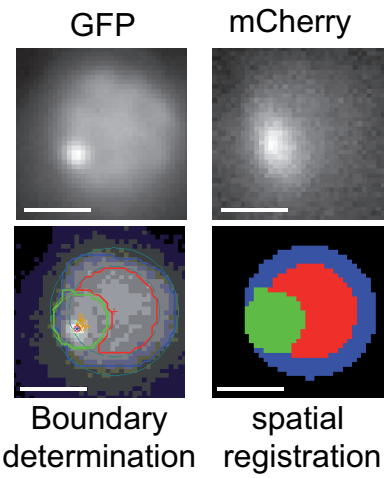

E

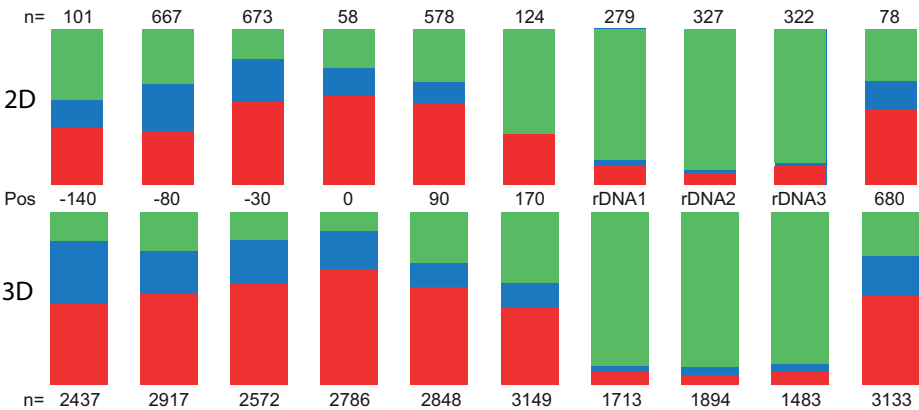

Supplementary figure 2 - Albert et al.,

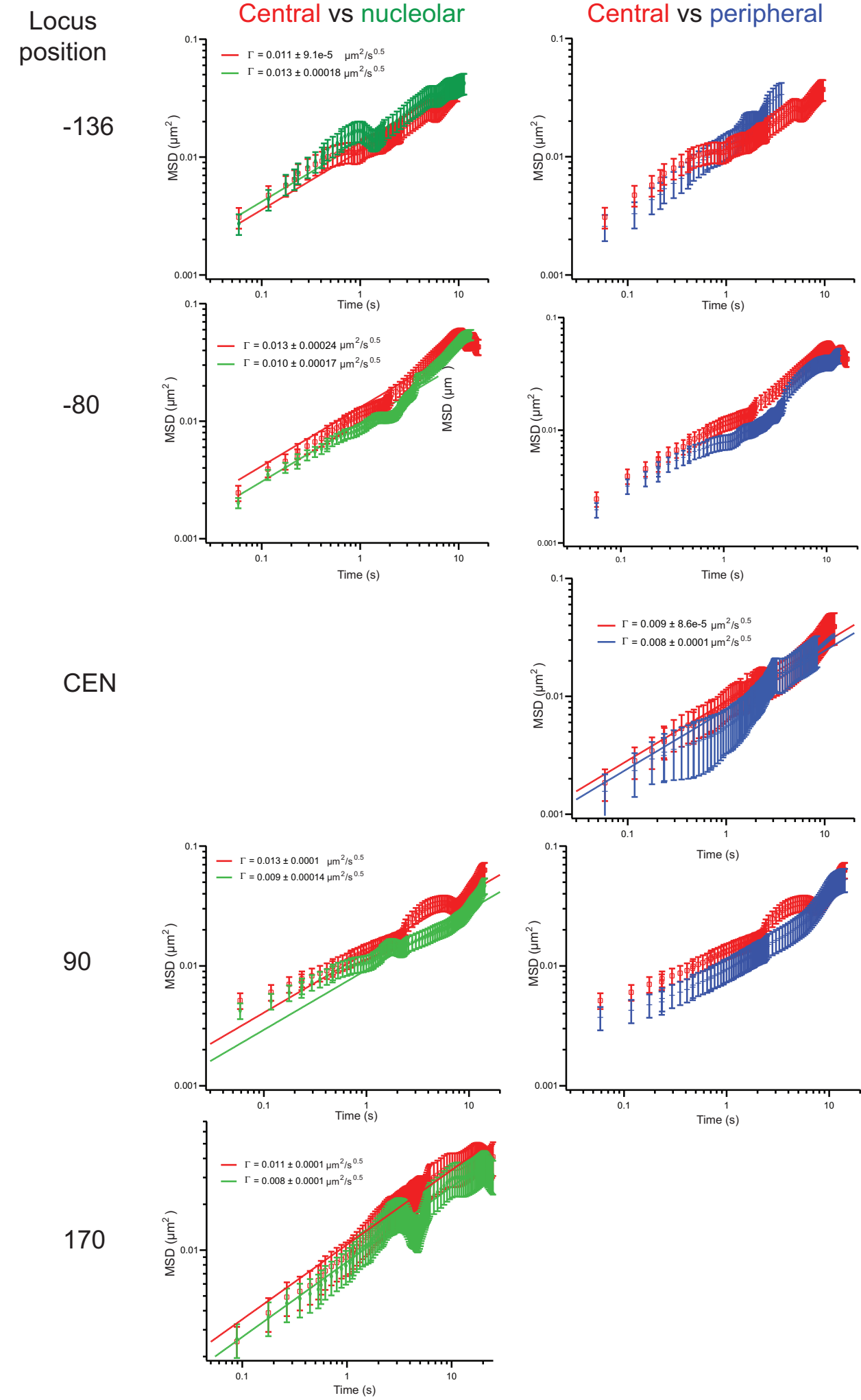

Supplementary Figure S3 - Albert

Legends for supplementary figures:

Movie 1: **Overlay of color-coded statistical mapping of loci positions along chromosome XII**. The spatial distributions of each locus are represented as a color-coded heat map determined by the percentile of the distribution (Berger et al., 2008; Therizols et al., 2010). The dashed yellow circle, the dashed red curve, and small red circle depict the median nuclear envelope, the median nucleolus, and the median location of the nucleolar center, respectively. Chromosome XII with the 12 fluorescent operator-repressor system (FROS) labeled loci is schematically represented using the centromere as origin (right panel). Time delay between each statistical mapping is proportional to distances in kb separating each locus. The overlay was generated using Adobe® After Effects® CS6.

Movie 2: **Interpolation between color-coded statistical maps of loci positions along chromosome XII**. Interpolation along the entire chromosome was achieved for each percentile color level independently, using *Adobe® After Effects® CS6* software. One statistical map with one kb resolution was then obtained for the entire chromosome, excluding rDNA.

Movie 3: Long term motion of one locus of chromosome XII in budding yeast. *S. cerevisiae* strain (HBT24-1a) bears one labeled locus (position 90 kb), a GFP tagged nuclear pore complex labeling nuclear envelop (Nup49-GFP) and a red nucleolar marker (mCherry-Nop1). Images were acquired by time-lapse microscopy, using a widefield microscope (Ti-E/B, Nikon Inc.). Frames for GFP were taken every 10s. Brightfield and mCherry signals were acquired every 100s. For visualization purposes, red and bright field images were refreshed every 10 GFP frames. Movie was set to 24 images per second, resulting in an apparent 240-times speed increase. Note that nuclear size increases with cell cycle progression, and nuclei move rapidly during mitosis. Images were processed for visualization (see material and methods).

Figure S1: Nuclear morphology of the 31 populations analyzed encompassing 15 FROS tagged strains in exponentially growing cells, 10 FROS strains rapamycin treated for 20 min, and four exponentially growing strains bearing FROS labeled Pol III transcribed genes along yeast chromosome XII. **A** Schematic representation of nuclear radius and distances separating nuclear and nucleolar centers in the cell population measured in 3D using the genemap method (Berger et al., 2008). Boxplot of nuclear radius (**B**) and distance between nuclear-nucleolar centers (**C**) in each of the 31 populations analyzed are shown. Nuclear morphology is comparable in each cell population, except for an increase in nuclear-nucleolar center distances when rapamycin treatment is applied

Figure S2: Tracking loci in living cells. **(A-C)** Signal-to-noise (SNR) ratio determination allows correction of measured mean square displacements (MSD). (**A)** Measurement of the tracking error in our custom-made software using simulated point-like structures. Point-like structures of defined positions and controlled SNR were generated *in silico* (simulated image; left part). Scale bar = 1 μm. The middle panel shows the intensity signal along the blue line represented on left image (blue curve, the pixel size is 80.5 nm), and the black curve is a Gaussian fit. The quadratic localization errors are plotted as a function of the SNR in the right panel (the line is a guide to the eye). (**B)** In the table, the measured SNR from time-lapse acquisition is reported for each locus, and for fast (60 ms) or slow (200 ms) interframe acquisitions. (**C**) We show for locus -136 the process flow for mean square displacement (MSD) analysis, starting from raw data (upper left graph). We then compensate for the difference in SNR by adding an error to the slow acquisition MSD dataset (as measured in A, right graph), which is determined by the difference in tracking precision. Datasets are then fused (lower left panel), and filtered using a Gaussian smoothing (order 11; lower right

panel). The resulting dataset is adjusted with an anomalous diffusion model (black line). **D** Spatial registration of cell nucleus. For time lapse acquisition of each nucleus (upper left panel), the nucleus is automatically segmented to define central, peripheral, and nucleolar regions, respectively red, blue, green. Two-color imaging of GFP signal at the left and the mCherry-Nop1 signal at the right, is used for segmentation (upper panel). These signals were segmented using an automatic contour detection based on threshold, and the resulting shapes were fitting with a circle (green, red and blue outlines). We then defined three nuclear regions: the nucleolus, which consisted in the region delimited by a circle of 1.1*nucleolus radius; the nuclear periphery which consisted in the region located beyond 31% of the nuclear radius and the nuclear center which was the region located at a distance to the periphery smaller than 31% of the nuclear radius (right panel). We also disregarded cells with nuclear anomalous shapes. (**E**) Spatial registration allows an unbiased sampling of gene trajectory in each nuclear region. Proportion of trajectory found in nucleolar, central or peripheral nuclear sub-compartment is compared with loci position determined in 3D. The distribution in each region is represented for 10 loci using the tracking software (upper panel, 2D). The lower panel depicts 3D loci localization in each cell population using genemap method (Berger et al., 2008). When using genemap (Berger et al., 2008), coordinates of a locus, the nucleolus (NUC) and the nuclear envelop (NE) are determined. Loci are considered nucleolar when positioned within 100 nm from segmented NUC, peripheral if at less than 100 nm from the NE, otherwise central. This tool allowed us to collect robust statistics from 50 to 500 cells.

Figure S3: MSD responses for loci -136, -80, CEN, 90 and 170 kb along chromosome XII.
In the left panel, we plotted the MSD response for a central or a nucleolar localization (red and green datasets, respectively). The same plot for a central and a peripheral localization is shown in the right panel (red and blue dataset, respectively). These data were adjusted with an

anomalous diffusion model with one adjustable parameter in $\Gamma t^{0.5}$. Note that the MSD datasets for genes located at -30, 680 kb and in the rDNA are represented in Figure 4. Nucleolar and peripheral trajectories were not obtained for respectively loci CEN and 170.

Supplementary references :

Berger, A.B., G.G. Cabal, E. Fabre, T. Duong, H. Buc, U. Nehrbass, J.C. Olivo-Marin, O. Gadal, and C. Zimmer. 2008. High-resolution statistical mapping reveals gene territories in live yeast. *Nat Methods*. 5:1031-1037.

Supplementary table S1 : Yeast strains				
FROS position/ Gen. position	FROS position/ CEN as origin	Name	genotype	Origine
WT	WT	**ODN1-1a**	*MATa his3Δ1 leu2Δ0 met15Δ0 ura3Δ0 trp1Δ0*	This study
		Nucloc2	*MATα his3Δ0 leu2Δ1 ura3-Δ851 ade2-801 lys2-Δ202::GFP::TETR-LYS2 nup49Δ::HPHMX3* + pASZ11-NupNop	(Berger et al., 2008)
untagged	untagged	**TMS1_1a**	*MATa* his3-Δ1, leu2-Δ1, ura3-Δ0, ade2-801, lys2-801,LYS2::TETR-GFP, nup49-Δ::HPH-MX6 + pASZ11-NupNop	Offspring of ODN1-1a x NucLoc2
Chr XII -014 kb	Chr XII -136 kb	**Ben1_2a**	*MATa his3-Δ1, leu2-Δ1, ura3-Δ0, ade2-801, lys2-801,LYS2::TETR-GFP, nup49-Δ::HPH-MX6, interPAU18-AYT1::his3::TetO-NAT* + pASZ11-NupNop	This study
Chr XII 070 kb	Chr XII – 80 kb	**Jez15_1a**	*MATa his3-Δ1, leu2-Δ1, ura3-Δ0, ade2-801, lys2-801,LYS2::TETR-GFP, nup49-Δ::HPH-MX6, interGRC3-RIX7::ura3::TetO-NAT* + pASZ11-NupNop	This study
Chr XII 120 kb	Chr XII – 30 kb	**ICH5_1a**	*MATa* his3-Δ1, leu2-Δ1, ura3-Δ0, ade2-801, lys2-801,LYS2::TETR-GFP, nup49-Δ::HPH-MX6, *interYLL014w-YLL013c::tetO-NAT* + pASZ11-NupNop	This study
Chr XII 150 kb	Chr XII 0 kb	**Jez11_1a**	*MATa his3-Δ1, leu2-Δ1, ura3-Δ0, ade2-801, lys2-801,LYS2::TETR-GFP, nup49-Δ::HPH-MX6, interDNM1-cen::his3::TetO-NAT* + pASZ11-NupNop	This study
Chr XII 240 kb	Chr XII 90 kb	**HBT24_1a**	*MATa* his3-Δ1, leu2-Δ1, ura3-Δ0, ade2-801, lys2-801,LYS2::TETR-GFP, nup49-Δ::HPH-MX6, *interYLR048W-YLR049C::his3::TetO-Nat* + pASZ11-NupNop	This study
Chr XII 320 kb	Chr XII 170 kb	**Ben3_1a**	*MATa his3-Δ1, leu2-Δ1, ura3-Δ0, ade2-801, lys2-801,LYS2::TETR-GFP, nup49-Δ::HPH-MX6, interYLR092w-YLR093c::his3::TetO-NAT* + pASZ11-NupNop	This study
Chr XII 420 kb	Chr XII 270 kb	**HBT27_1a**	*MATa* his3-Δ1, leu2-Δ1, ura3-Δ0, ade2-801, lys2-801,LYS2::TETR-GFP, nup49-Δ::HPH-MX6, *interYLR143w-YLR144c::ura3::TetO-Nat* + pASZ11-NupNop	This study
Chr XII 530 kb	Chr XII 380 kb	**Jez14_1a**	*MATa his3-Δ1, leu2-Δ1, ura3-Δ0, ade2-801, lys2-801,LYS2::TETR-GFP, nup49-Δ::HPH-MX6, interYLR188w-YLR189c::ura3::TetO-NAT*+ pASZ11-NupNop	This study
Chr XII 610 kb	Chr XII 460kb	**HBT28_1a**	*MATa* his3-Δ1, leu2-Δ1, ura3-Δ0, ade2-801, lys2-801,LYS2::TETR-GFP, nup49-Δ::HPH-MX6, i*nterYLR238W-YLR239C::his3::TetO-Nat* + pASZ11-NupNop	This study
Chr XII 740 kb	Chr XII 590 kb	**Ben5_1a**	*MATa his3-Δ1, leu2-Δ1, ura3-Δ0, ade2-801, lys2-801,LYS2::TETR-GFP, nup49-Δ::HPH-MX6, interYLR307w-YLR307c-a::his3::TetO-NAT* + pASZ11-NupNop	This study
Chr XII 830 kb	Chr XII 680 kb	**Jez1_1a**	*MATa his3-Δ1, leu2-Δ1, ura3-Δ0, ade2-801, lys2-801,LYS2::TETR-GFP, nup49-Δ::HPH-MX6, interYLR353w-YLR354c::his3::TetO-NAT* + pASZ11-NupNop	This study
Chr XII 1030 kb	Chr XII 880 kb	**HBT30_1a**	*MATa* his3-Δ1, leu2-Δ1, ura3-Δ0, ade2-801, lys2-801,LYS2::TETR-GFP, nup49-Δ::HPH-MX6, *interYLR451w-YLR452c::his3::TetO-NAT* + pASZ11-NupNop	This study
ChrXII-rDNA1	ChrXII-rDNA	**Ben51_1a**	*MATa his3-Δ1, leu2-Δ0, C, ura3-Δ0, ade2-801, lys2801,LYS2::TETR-GFP, nup49-Δ::HPH-MX6 inter rDNA ura3::TetO-NAT+ pASZ11-NupNop*	This study
ChrXII-rDNA2	ChrXII-rDNA	**Ben52_1a**	*MATa his3-Δ1, leu2-Δ0, C, ura3-Δ0, ade2-801, lys2801,LYS2::TETR-GFP, nup49-Δ::HPH-MX6 inter rDNA ura3::TetO-NAT+ pASZ11-NupNop*	This study
ChrXII-rDNA3	ChrXII-rDNA	**Ben57_1a**	*MATa his3-Δ1, leu2-Δ0, C, ura3-Δ0, ade2-801, lys2801,LYS2::TETR-GFP, nup49-Δ::HPH-MX6 inter rDNA ura3::TetO-NAT+ pASZ11-NupNop*	This study
SNR6	Chr XII 210 kb	**yCNOD15-1c**	*MATa* his3-Δ1, leu2-Δ0, ura3-Δ0, ade2-801, lys2-801,LYS2::TETR-GFP, nup49-Δ::HPH-MX6 interSNR6-YLR108c::his3::tetO-NATMX6 + pASZ11-NupNop	This study
tP(UGG)L	Chr XII -60 kb	**yCNOD123-1a**	MATa his3-Δ1, leu2-Δ1, ura3-Δ0, ade2-801, lys2-801,LYS2::TETR-GFP, nup49-Δ::HPH-MX6, inter tP(UGG)L-PAU17::his3::TetO-Nat + pASZ11-NupNop	This study
tA(UGC)L	Chr XII 60 kb	**yCNOD124-1a**	MATa his3-Δ1, leu2-Δ1, ura3-Δ0, ade2-801, lys2-801,LYS2::TETR-GFP, nup49-Δ::HPH-MX6, inter tA(UGC)L-MLH2::ura3::TetO-Nat + pASZ11-NupNop	This study
tL(UAA)L	Chr XII 810 kb	**yCNOD125-1a**	MATa his3-Δ1, leu2-Δ1, ura3-Δ0, ade2-801, lys2-801,LYS2::TETR-GFP, nup49-Δ::HPH-MX6, inter tL(UAA)L-YLR419w::ura3::TetO-Nat + pASZ11-NupNop	This study

Supplementary table S2

number	Name	Genomic position	sequence
558	chrXII-014K-M13F	interPAU18-AYT1	AATTTCATCGTCTTATATTTCGATAATAAAACAATACAGTGAGCGTTGTTATTAAGTAAATCATAGGCACTTGGTATCATGTAAAACGACGGCCAGT
559	chrXII-014K- M13R	interPAU18-AYT1	TCAATAAGGAGATGAACTAGGCCATCAACAATTACTAACACGCACACACGCACTACTACAACTACTTGATTTTGAATTATGGAAACAGCTATGACCATG
610	o-chrXII-70k-M13F	interGRC3-RIX7	CGTCATGAGACGTGGCCAATTCATGAAAAGATAGAAAGAAAAGGTAATCGTACATTTTTTAATAGTGAAAGATAGAGGATACAGTAAAACGACGGCCAGT
611	o-chrXII-70k-M13R	interGRC3-RIX7	GTCCCTAGAAGTTAGTATGACTTAGATATTGAAGGAATATGAGTATACATAACAAATATATAAAACTTTGCATGATTTTTGGGAAACAGCTATGACCATG
560	o-chrXII120k	interYLL014W-YLL013C	ACATGACAACAGTATTCTCAGTCAAATGATTTCAAATACACAATGTTAAATTCTCTATCTGTTGCAGAAATAAGAAGAGCGTAAAACGACGGCCAGT
561	o-chrXII120k-rev	interYLL014W-YLL013C	ATATTCATTATTTGCTTTTTTCCATTACCTACTTTTTGTACCTCATCTCTATTTTTCTGCAAAAATCTTTGCGCTCTTACGGAAACAGCTATGACCATG
606	o-chrXII150k-M13F	interDNM1-cen	TTATAGGTCAGTGTTTATTCCTTTACTCAGTTGATGATTTCAAATGTGCTCTCCTCTCCATTCTTTTTCTTGTTAATAAAAATGTAAAACGACGGCCAGT
607	o-chrXII150k-M13R	interDNM1-cen	GGTAGAGCTTCTCTAGTGAAGGTTCTCTAGCTTAGTTAATACTTTTGCGATTGCTAATATTTGTTATTTATTTAGTTATGGGGAAACAGCTATGACCATG
562	o-chrXII24k	interYLR048W-YLR049C	TTTTTTATTAGGTAAGTGGTTTCAATAATTAAATTCTTTAGCGGGAAGGCTGACTATCTATAGTATTGAAGATAAGTTAAGTAAAACGACGGCCAGT
563	o-chrXII24krev	interYLR048W-YLR049C	AATACTCGGGTGAACCCGTCATGGCGAATAGTGCAAATTTAATTAATAATAAAAATGAAATATCAGAACTAAACATTAATGGAAACAGCTATGACCATG
564	o-chrXII32k	interYLR092W-YLR093C	TCATAATGAGATAGACACTGTTTATATAATAAGAAATAATAGGTAGGATGGTGCCATCGTGAGCATATACATACCTATAAGTAAAACGACGGCCAGT
565	o-chrXII32krev	interYLR092W-YLR093C	ACGACAATAACATTAATAACGGTTGTATTTCTTTTGTTCCTGAGAGGAAGAGAAAAATAAAATAAAAATAAGGTAAATATGGAAACAGCTATGACCATG
566	o-chrXII42k	interYLR143W-YLR144C	ATACGCTGTCCACGCTCCTGGCGGTGTAAATGATAGACAGATCCCAAATATGTTAGCAAATCATAGGAACAACACCATATGTAAAACGACGGCCAGT
567	o-chrXII42krev	interYLR143W-YLR144C	TCCTAAACCATCATCAATAATCAAATTATTACAGAACACACCTTAATTGTGCGGCGTATTCTAAATTTTACGTGTTCACAGGAAACAGCTATGACCATG
568	o-chrXII53k	interYLR188W-YLR189C	TCCTTGTACGCCTTTATACACATTAAATTAATATTAGATGCACAACATACGGTACGTTTAGGAAACTCAAATTAAGCTTTAGTAAAACGACGGCCAGT
569	o-chrXII53krev	interYLR188W-YLR189C	AAGTTTCAGTCATATTTGTACTCAGGAAAGATATGAAAACGATAATGTTGATAATAAGAATAATAGTAACAATAATGGAAACAGCTATGACCATG
570	o-chrXII61k	interYLR238W-YLR239C	TTTCCCCCAACTAGCATCGTAAATACAAGACACACACGATCCGCTTTTCACGTCAGAGATTATTATATACGTACGTATATGTAAAACGACGGCCAGT
571	o-chrXII61krev	interYLR238W-YLR239C	TCCGTGAGACGGATGACTCCCCCCATACTTTCTTAAATGAAAGGATGCTTACCTTTTTTTACATGTGAATATCTATTACATGGAAACAGCTATGACCATG
572	o-chrXII74k	interYLR307W-YLR307C-A	AGTATGTATTAGAATAGAGGACATATATAAAAATCATATATATCGATGCTTGAATGTATAAGGAAAAGCGTCAAATTATGGTAAAACGACGGCCAGT
573	o-chrXII74krev	interYLR307W-YLR307C-A	CTAAAAGATTCTAAAAAATTACTTTTTAAAGTTATACCCTCTGACTTTATGTGACATCAGCATCCTAAGTACCTACCGTTGGAAACAGCTATGACCATG
574	o-chrXII83k	interYLR353W-YLR354C	AAACTGTTCTGTCTCGTTAAAGTCATATATATAAATAGGGGATTTTCATTAATTTATATATATAGATATACTTGTGTACAGTAAAACGACGGCCAGT
575	o-chrXII83krev	interYLR353W-YLR354C	TTACCGCTTAAGGAAGTATCTCGGAAATATTAATTTAGGCCATGTCCTTATGCACGTTTCTTTTGATACTTACGGGTACAGGAAACAGCTATGACCATG
576	o-chrXII1030k	interYLR451W-YLR452C	CAGACGGACTTAAACCGCCAACCAGCCTTGGCCACAGGTGTATGATGCGAAGATTCGTAAGCGCTCACGTTAGTCACATCGTAAAACGACGGCCAGT
577	o-chrXII1030krev	interYLR451W-YLR452C	AGCGGAGGTGTGATTTGTTATATCAACTATAATATGATTAAATAAAGCCATTTATTATCTAGTATAATTTCCAATCCTGAGGAAACAGCTATGACCATG
1033	URA3_M13F-SceI	Construction of SI-SceI-URA3.	aaaaaaggatccggtatcgataagcttgatGTATTACCCTGTTATCCCTAGCGTATGTGGCTGTGGTTTCAGGGTCCAT
1034	URA3_M13R	Construction of SI-SceI-URA3.	tttttgtcgaccccgggctgcaggaattcgatTGT
1035	rDNA-M13F.	Tagging of rDNA.	AGCAGTTTTTTCCGCACCATCAGAGCGGCAAACATGAGTGCTTGTATAAGTTTAGAGAATTGAGAAAAGCTCATTTCCTATAGGTAAAACGACGGCCAGT
1036	rDNA-M13R	Tagging of rDNA.	TCACTGTTCACTTGTCTCTTACATCTTTCTTGGTAAAATCGTAGTTCGTAGTATTTTTTTTCATATCAAAGGCATGTCCTGGGAAACAGCTATGACCATG
528	o-M13F_SNR6	interSNR6-YLR108c	TGAATGTGAATATTGTTACAGCTATGCAATGGTACGATCATACTCTGAACGATCCATTTAAATTATATATGTAAAACGACGGCAGT
529	o-M13R_SNR6	interSNR6-YLR108c	GAAGGAATATTGCAAAATGATTGATTTTCTGTGAAATCTTCAATAAAAAAACCTTTCTCTTCTGTTTGACGGAAACAGCTATGACCATG
1240	tP(UGG)L-rev	inter tP(UGG)L-PAU17	GCACAAACTGAGGATTCTCAGCCTTCCTACGGCATAATCCTTTATAATTATTGTTTTAGCCCAGGAAACAGCTATGAC
1241	tP(UGG)L_fw	inter tP(UGG)L-PAU17	TTACAACTAATGGTATGCAATTCATAAAGCATAGGCCAAAAGACCCTGATACAGATATATGTAAAACGACGGCCAGT
1244	tA(UGC)L-fw	inter tA(UGC)L-MLH2	ACAGTAAAAGCAAAAAAGCATTGTGCCAGGGCAATATAGCGAGCACTACTTAAACCCAAAGTAAAACGACGGCCAGT
1245	tA(UGC)L-rev	inter tA(UGC)L-MLH2	GATTACCTTCTGCATTATCTATAAGTTTTGCGCATAACAAACCTTTCACTTGTCACCTAACCAGGAAACAGCTATGAC
1250	tL(UAA)L-rev	inter tL(UAA)L-YLR419w	AAAGACAATGTGCTATGTAGTTTACGGGATTCTAGCCCTGATTCAGCAAAGAGAAAAACACCAGGAAACAGCTATGAC
1251	tL(UAA)L-fw	inter tL(UAA)L-YLR419w	CATATAGAAGTGTCAAAGTATAAAACACTAACAAAAATCTAAGAGATTATTGCGACTGCGGTAAAACGACGGCCAGT
	SNR6_HindIII_F	Probe for IEL	AGCTTTAAAGGCTCTGATTTTGGATTCG
	SNR6_HindIII_R	Probe for IEL	CACAGCATGGATACTGATGGTTCTTGGT
	SNR6	Oligo For RT (98 pb product)	TCTCTTTGTAAAACGGTTCATCCT

	SNR14 (U4 control)	Oligo For RT (115 pb product)	GCGAACACCGAATTGACCATG

Supplementary table S3

Nom	Référence
pTetO-Nat-HIS3Δ	(Berger et al., 2008)
pTetO-Nat-URA3Δ	(Berger et al., 2008)
pCR4-HIS3-M13	(Berger et al., 2008)
pSK-URA3-M13	(Berger et al., 2008)
pASZ11-GFP-NUP49-NOP1-Cherry	(Berger et al., 2008)
pSK-URA3-SceI-M13	This study

Berger, A.B., G.G. Cabal, E. Fabre, T. Duong, H. Buc, U. Nehrbass, J.C. Olivo-Marin, O. Gadal, and C. Zimmer. 2008. High-resolution statistical mapping reveals gene territories in live yeast. *Nat Methods*. 5:1031-1037.